Acta Crystallographica Section D
Biological Crystallography
ISSN 0907-4449

Glass transition in thaumatin crystals revealed through temperature-dependent radiation-sensitivity measurements

Matthew Warkentin* and Robert E. Thorne

Physics Department, Cornell University, Ithaca, New York, USA

Correspondence e-mail: maw64@cornell.edu

Received 12 July 2010
Accepted 3 September 2010

The temperature-dependence of radiation damage to thaumatin crystals between T = 300 and 100 K is reported. The amount of damage for a given dose decreases sharply as the temperature decreases from 300 to 220 K and then decreases more gradually on further cooling below the protein-solvent glass transition. Two regimes of temperature-activated behavior were observed. At temperatures above ∼200 K the activation energy of 18.0 kJ mol^{-1} indicates that radiation damage is dominated by diffusive motions in the protein and solvent. At temperatures below ∼200 K the activation energy is only 1.00 kJ mol^{-1}, which is of the order of the thermal energy. Similar activation energies describe the temperature-dependence of radiation damage to a variety of solvent-free small-molecule organic crystals over the temperature range T = 300–80 K. It is suggested that radiation damage in this regime is vibrationally assisted and that the freezing-out of amino-acid scale vibrations contributes to the very weak temperature-dependence of radiation damage below ∼80 K. Analysis using the radiation-damage model of Blake and Phillips [Blake & Phillips (1962), *Biological Effects of Ionizing Radiation at the Molecular Level*, pp. 183–191] indicates that large-scale conformational and molecular motions are frozen out below T = 200 K but become increasingly prevalent and make an increasing contribution to damage at higher temperatures. Possible alternative mechanisms for radiation damage involving the formation of hydrogen-gas bubbles are discussed and discounted. These results have implications for mechanistic studies of proteins and for studies of the protein glass transition. They also suggest that data collection at $T \simeq 220$ K may provide a viable alternative for structure determination when cooling-induced disorder at T = 100 is excessive.

1. Introduction

Studies of biological matter using ionizing radiation must contend with the problem of radiation damage. Even under ideal experimental conditions, radiation damage places fundamental limits on the amount of information that can be obtained from each sample.

Radiation damage is critical when determining protein and virus structures by X-ray or electron crystallography (Blake & Phillips, 1962; Hendrickson, 1976; Nave & Garman, 2005; Holton, 2009). X-rays rapidly damage crystals held at room temperature. The incident X-ray fluence and the corresponding dose required to determine a molecular structure are typically much larger than those required to severely degrade the diffraction of the crystal. In the early days of protein crystallography this problem was overcome by using very

large crystals and/or by scaling together diffraction data obtained from many crystals.

Following the development of reliable cryocrystallography protocols in the 1990s (Hope, 1988; Rodgers, 1994; Garman & Schneider, 1997), most diffraction data have been collected at temperatures near T = 100 K. At these low temperatures protein crystals are typically 50–100 times less sensitive to X-rays than at T = 300 K (Nave & Garman, 2005; Southworth-Davies *et al.*, 2007). They continue to yield structurally useful diffraction for doses (depending upon the definition of useful) as large as ∼20–30 MGy (Teng & Moffat, 2000, 2002; Nave & Garman, 2005; Owen *et al.*, 2006; Kmetko *et al.*, 2006), which is consistent with experience in cryoelectron microscopy (Henderson, 1990). However, improved X-ray sources, optics and detectors now allow low-background diffraction data collection from micrometre-size crystals (see, for example, Coulibaly *et al.*, 2007). Radiation-damage limits at T = 100 K (Holton & Frankel, 2010) are once again requiring the merging of data from multiple crystals.

Furthermore, there are many reasons to collect diffraction data at higher temperatures. T = 100 K data from cryoprotected crystals provide no information about conformational changes that occur on cooling from biological temperatures or that may be induced by cryoprotectants (Charron *et al.*, 2002). Many biologically important targets, including large complexes and viruses, can be difficult to flash-cool without introducing excessive disorder. Dramatic changes in protein dynamics associated with the protein-solvent glass transition (Parak *et al.*, 1982; Doster *et al.*, 1989; Tilton *et al.*, 1992; Rasmussen *et al.*, 1992) occur near T = 200 K. Mechanistic studies of protein function require measurements at temperatures at which substrates can be diffused in and out and at which the conformational dynamics resemble those at biological temperatures.

As a result, radiation damage at temperatures spanning the full range T = 300–100 K remains a major issue in structural biology (Weik & Colletier, 2010). The mechanisms by which X-rays degrade diffraction quality throughout this temperature range remain poorly understood.

1.1. Radiation-damage phenomenology

Radiation damage caused by X-ray absorption and inelastic scattering can be crudely separated into global and site-specific components. Global damage involves atomic displacements whose distribution is essentially random within the unit cell. The crystal's diffraction-peak intensities then decay more or less uniformly with scattering angle, producing a spatially uniform loss of resolution in the electron-density map. However, some sites within the unit cell, such as those involving weak bonds, may be much more easily and frequently damaged than others. These regions may change their conformations in a consistent way, modulating the relative intensities of diffraction peaks and producing site-specific changes in electron density that can be easily recognized long before appreciable global damage has accumulated (Weik *et al.*, 2000; Burmeister, 2000; Leiros *et al.*, 2001, 2006). Although dominated by random changes, practical measures of global damage such as the overall B factor or diffraction resolution are also weakly modulated by site-specific changes.

At T = 100 K the overall B-factor metric of global damage varies linearly with dose (except perhaps at very large doses). For a given dose it is relatively constant (within a factor of two) for a variety of different protein crystals (Owen *et al.*, 2006; Kmetko *et al.*, 2006; Holton, 2009) and is independent of the dose rate (Leiros *et al.*, 2001, 2006; Ravelli *et al.*, 2002; Sliz *et al.*, 2003; Shimizu *et al.*, 2007), which is consistent with observations in cryoelectron microscopy (Henderson, 1990).

In contrast, the types and extent of site-specific damage vary greatly from protein to protein (Weik *et al.*, 2000, 2001; Burmeister, 2000). Site-specific damage can both complicate phasing (Ravelli & McSweeney, 2000) and, by introducing dose-dependent anomalous differences, provide an alternative approach to phasing (Ravelli *et al.*, 2003, 2005). Site-specific damage has proven to be useful in kinetic crystallography, in which X-rays can be used to drive a reaction in the active site of an enzyme (Schlichting *et al.*, 2000; Bourgeois & Royant, 2005; Colletier *et al.*, 2008).

1.2. Radiation-damage mechanisms

What are the mechanisms responsible for X-ray radiation damage to protein crystals and how do the dominant mechanisms evolve with temperature? Based on studies in other organic and biological systems, damage is believed to involve two phases, called 'primary' and 'secondary' (Teng & Moffat, 2000). In the primary phase, an X-ray photon with energy ≃10 keV is absorbed or inelastically scattered by a protein or solvent atom, depositing a large amount of energy. A shower of ∼10–100 eV secondary electrons (Singh & Singh, 1982; Cowan & Nave, 2008) carries this energy away, generating a cascade of radiochemical reactions and additional photoelectrons within a range of ∼3 µm of the initial hit (Cole, 1969; Nave & Hill, 2005; Holton, 2009). Free radicals are generated in the solvent, excited electrons move along the protein backbone and bonds are broken within the protein. All of this occurs on sub-nanosecond timescales that are faster than diffusive atomic motions (Henderson, 1995). As a result, these primary-damage processes are expected to be relatively temperature-independent.

In the secondary-damage phase, free radicals diffuse through the solvent and react with the protein, causing additional damage and producing additional radicals. As local damage accumulates, larger regions of each molecule may be destabilized and change their conformation and may cause the molecule to rotate and displace within the crystal lattice. Eventually, the molecule may become amorphous and cease to contribute to the Bragg diffraction (Blake & Phillips, 1962). Because many of the processes of secondary damage require diffusive motions of ions, atoms or atomic assemblies, they are expected to be strongly temperature-dependent. Little secondary damage should occur at very low temperatures, where diffusion is frozen out and the frozen solvent network provides a scaffold that inhibits protein conformational

changes and displacements. Note that there are alternative divisions of radiation-damage processes into primary and secondary phases (Garman, 2010); the present division follows Teng & Moffat (2000) and the radiation-damage literature for DNA and inorganic materials.

Here, we describe measurements and modeling of the temperature-dependence of global radiation damage that provide insight into the mechanisms of secondary damage, as well as radiation-sensitivity data that are essential for the design of future variable-temperature crystallographic studies of protein structure and dynamics. Using the radiation-damage metric of Kmetko *et al.* (2006), we examined 49 thaumatin crystals to determine the radiation-sensitivity at 11 temperatures from 300 to 100 K. Our results agree with previous studies at 300 and 100 K and indicate that most of the reduction in sensitivity on cooling from 300 to 100 K occurs above 200 K. These results are consistent with previous reports on the temperature-dependence of global damage (Teng & Moffat, 2002; Borek *et al.*, 2007; Meents *et al.*, 2010). We model radiation damage as a thermally activated process with a large barrier and a small barrier. The large barrier of 18.0 ± 2.9 kJ mol^{-1} dominates above 200 K and agrees with the activation energies for diffusion of radical species, diffusion of protein-hydration water and protein conformational motions, which are processes that are believed to be important in secondary damage. The small barrier dominant below 200 K is consistent with temperature-dependent radiation-sensitivity measurements on small-molecule organic compounds ($\sim$1.00 $\pm$ 0.33 kJ mol^{-1}) and is comparable to the excitation energies for amino-acid-scale vibrations.

Finally, we show that the 'reaction pathway' by which damage proceeds has a sensible temperature-dependence. Following Blake & Phillips (1962), we model radiation damage to protein crystals as a three-state process in which undamaged protein can become disordered or completely disrupted (amorphous) and use our data to determine the 'rate constants', which are proportional to the number of transitions between each state per unit dose. We find that the process is sequential: protein is first disordered and then becomes amorphous. Below $T = 200$ K the rate for disordering is 2.5 times larger than that for amorphization, which is consistent with a previous $T = 100$ K study (Sliz *et al.*, 2003). As the temperature is increased above $T = 200$ K amorphization plays an increasingly important role and at $T = 300$ K the amorphization and disordering rates are equal. This is consistent with the notion that large-scale conformational and molecular motions are frozen out below $T = 200$ K and become increasingly prevalent at higher temperatures, where they make a relatively larger contribution to the overall loss of crystal order.

2. Methods

2.1. Crystallization

Tetragonal thaumatin crystals were grown in 24-well trays using the hanging-drop method. Purified thaumatin powder (Sigma–Aldrich, St Louis, Missouri, USA) was dissolved to a concentration of 25 mg ml^{-1} in 100 m*M* potassium phosphate buffer pH 6.8 and a well solution was prepared by adding 1 *M* sodium potassium tartrate to the same buffer. 10 µl drops prepared by mixing 5 µl each of protein and well solution were suspended over 500 µl well solution. No penetrating cryoprotectants were added to the crystals at any temperature and a thorough wash in oil (as described in Warkentin & Thorne, 2009) was sufficient to obtain satisfactory cryocooling.

2.2. Crystal mounting

For data collection at temperatures below $T = 270$ K, each crystal was first transferred from its growth drop or a cryoprotectant solution into thick immersion oil (NVH oil, Cargille Labs, Cedar Grove, New Jersey, USA). MicroTools, Micromounts (MiTeGen, Ithaca, New York, USA) and nylon CryoLoops (Hampton Research, Aliso Viejo, California, USA) were used to manipulate the crystal until all of the solvent clinging to its surface had been removed. The crystal was retrieved from the oil using a MicroMount and excess oil was removed to minimize sample motion and background X-ray scatter. The crystal-containing mount was then placed on the diffractometer's goniometer and flash-cooled to the desired temperature using a Cryostream 700 (Oxford Cryosystems, Oxford, England) cold nitrogen-gas stream cooler. For data collection at temperatures of 270 and 300 K, where the vapor pressure of water is appreciable, crystals were mounted in a large drop of immersion oil to prevent dehydration.

2.3. X-ray diffraction experiments

X-ray diffraction data were collected at the Cornell High Energy Synchrotron Source (CHESS) on MacCHESS stations A1 and F1 using X-ray energies of 12.6 keV (A1) and 13.5 keV (F1), 100 µm collimators and Quantum 210 (A1) and 270 (F1) CCD detectors (ADSC, Poway, California, USA). The incident X-ray flux was determined using a 6 cm nitrogen ionization chamber, whose measurements agreed with those using a calibrated PIN diode (Hamamatsu Photonics Part No. S3590-09, Bridgewater, New Jersey, USA) to within $\sim$10%.

During irradiation, consecutive sets of five data frames with an oscillation width per frame of 1° were collected. Because the crystals were larger than the X-ray beam, frames were collected from the same 5° wedge to ensure that each dose was delivered to the same crystal region. Crystal oscillation (rotation) increases the irradiated volume by a factor that depends on the length of the crystal along the beam and so reduces the average dose for a given flux. For our geometry, the effect is only 4% for a 200 µm length and 9% for a 400 µm length and is not included in the reported radiation-sensitivities. The number of crystals examined at each temperature was nine at 300 K, four at 270 K, three at 240 K, two at 220 K, two at 210 K, five at 200 K, two at 190 K, seven at 170 K, two at 150 K, seven at 130 K and six at 100 K, giving a total of 49.

2.4. Data processing

Each set of five frames was indexed and integrated independently using both *MOSFLM* (Collaborative Computational Project, Number, 1994; Leslie, 2006) and *DENZO* (Otwinowski & Minor, 1997). The total intensities within a given resolution shell were calculated by summing the integrated intensities of each reflection. The resulting total intensity *versus* dose curves generated by the two programs gave essentially identical half-dose values. Relative *B* factors between each frame set and the initial set were obtained using both *SCALEIT* (Howell & Smith, 1992; Collaborative Computational Project, Number, 1994) and *SCALEPACK* (Otwinowski & Minor, 1997) as described in Kmetko *et al.* (2006). Both programs gave similar results, except that the relative *B* factors from *SCALEPACK* were consistently 1.33 times larger than those from *SCALEIT*. The dose curves shown here were generated by *SCALEPACK*, but the coefficients of sensitivity were scaled down by 1.33 to match those from *SCALEIT* and allow comparison with Kmetko *et al.* (2006).

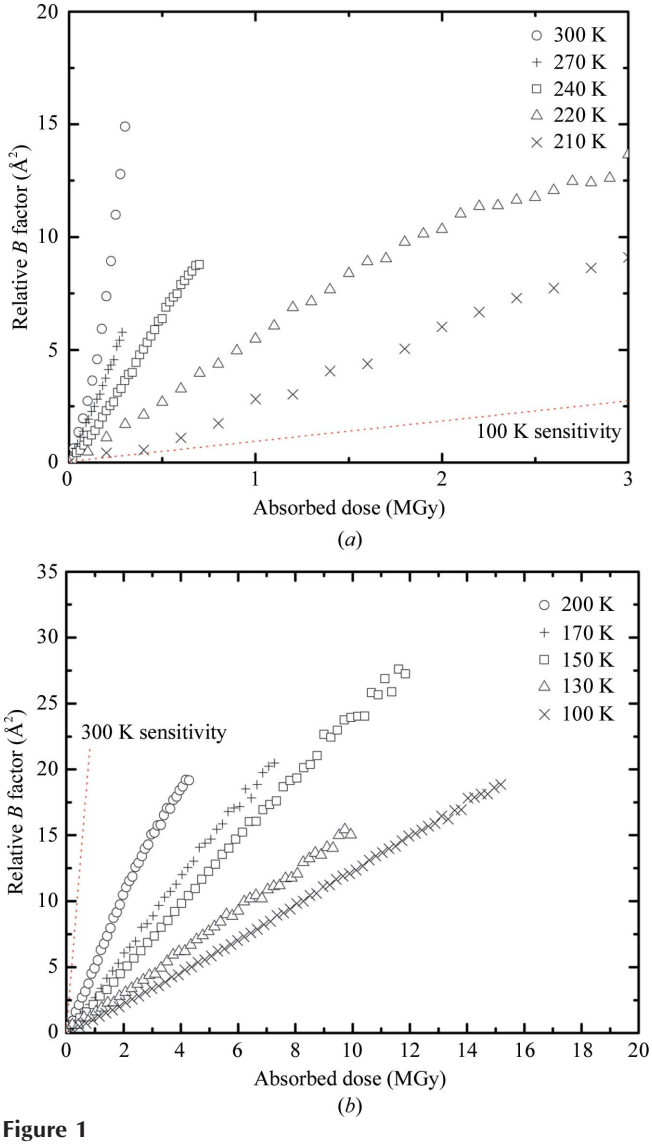

Figure 1
Representative data for relative *B* factor (characterizing the increase in disorder arising from radiation damage) *versus* X-ray dose obtained from thaumatin crystals at temperatures between (*a*) 300 and 210 K and (*b*) 200 and 100 K. Each curve represents data from a single thaumatin crystal. The dashed lines indicate the initial slopes of the data at $T = 100$ and 300 K, respectively. The high-temperature and low-temperature data are plotted on different dose scales because the *B*-factor increase with dose is roughly 50 times larger at $T = 300$ K compared with $T = 100$ K.

3. Results

Although many studies have examined radiation damage at room temperature and at temperatures below ∼180 K, temperature-dependent studies of radiation damage over the full temperature range between $T = 300$ and 100 K have not previously been attempted, in part because of the difficulty in collecting data between $T = 220$ and 180 K. At these temperatures water rapidly crystallizes and protein-crystal diffraction patterns develop ice rings and rapidly degrade (Tilton *et al.*, 1992). However, these temperatures are of the greatest interest for understanding radiation-damage mechanisms because near $T = 200$ K the protein and solvent system undergoes a dynamical/glass transition (Parak *et al.*, 1982; Doster *et al.*, 1989; Weik *et al.*, 2001, 2004, 2005; Gabel *et al.*, 2002).

The present study was made possible by the methods and observations described in detail by Warkentin & Thorne (2009), which were in turn inspired by earlier investigations (Weik *et al.*, 2001, 2005; Juers & Matthews, 2001, 2004; Kriminski *et al.*, 2002; Warkentin *et al.*, 2006). Ice nucleation within protein crystals is strongly suppressed because the solvent is confined within a nanoporous network (Rault *et al.*, 2003) and because much of the solvent is involved in hydrogen-bonding interactions with the protein. In contrast, the external solvent that typically surrounds a crystal rapidly crystallizes, dehydrating the crystal and perhaps also nucleating ice formation within it. By carefully and completely removing all of the external solvent, crystals of many proteins including thaumatin can be cooled to arbitrary temperatures without appreciable ice nucleation or degradation of diffraction properties and often without the addition of any penetrating cryoprotectants.

Relative *B* factor ($B_{\rm rel}$) *versus* dose curves for thaumatin crystals were determined at 11 temperatures between $T = 300$ and 100 K. Relative *B* factors provide a measure of global radiation damage and were obtained by scaling successive 5° data sets against the initial set, as described in Kmetko *et al.* (2006) (see §2). Fig. 1 shows representative dose curves at selected temperatures. At all temperatures, $B_{\rm rel}$ varies linearly with dose at small doses. Above $T \simeq 200$ K significant but somewhat erratic deviations from linearity are observed at large doses. At $T = 300$ K, for example, measurements on nine crystals revealed damage that appears to 'run away' (*i.e.* to abruptly increase until the diffraction is too disordered for analysis) beyond a sample-dependent dose, perhaps owing to plastic failure of the crystal caused by radiation-damage-induced internal stresses. Below $T \simeq 200$ K, the dose curves remain nearly linear out to much larger doses and $B_{\rm rel}$ values.

The slope of the B_{rel} *versus* dose curve in the linear/low-dose region divided by $8\pi^2$ gives a coefficient of sensitivity to absorbed dose (s_{AD}; Kmetko *et al.*, 2006). s_{AD} is (in a simple model) related to the mean-squared atomic displacements caused by irradiation. Fig. 2 shows s_{AD} *versus* inverse temperature. Each temperature point was obtained by averaging the slope of B_{rel} *versus* dose data at that temperature for several crystals; the error bars indicate the crystal-to-crystal variation.

The total reduction in radiation-sensitivity on cooling from $T = 300$ to 100 K is approximately a factor of 50. Much of this reduction occurs above $T = 200$ K; relative to $T = 300$ K, the sensitivity is reduced by factors of 10 and 15 (or by 90 and 93%) at 220 and 180 K, respectively.

If the rate-limiting step for radiation damage in a given temperature range is thermally activated (as is expected, for example, for diffusive motions) then the slope of the data on the Arrhenius axes in Fig. 2 should give the activation energy. The dotted and dashed lines in Fig. 2 suggest that there are two regimes between $T = 300$ and 100 K: a high-temperature regime with a large activation energy E_{a1} and a low-temperature regime with a small activation energy E_{a2}. The solid line in Fig. 2 is a composite fit,

$$s_{AD} = A_1 \exp(-E_{a1}/RT) + A_2 \exp(-E_{a2}/RT), \qquad (1)$$

where $E_{a1} = 18.0 \pm 2.9$ kJ mol^{-1} and $E_{a2} = \sim 1.00 \pm 0.33$ kJ mol^{-1}.

4. Discussion

4.1. The glass transition in radiation-sensitivity

Between $T = 300$ and 200 K, the activation energy of 18.0 kJ mol^{-1} dominates the radiation-sensitivity. This value is comparable to the values of 12–17 kJ mol^{-1} for diffusion-controlled reactions of solvated electrons, H and OH radicals with a wide variety of small molecules in solution (Anbar & Hart, 1967; Buxton *et al.*, 1988). This value is also comparable to the values of 17.33 and 14.57 kJ mol^{-1} for the translational diffusion of hydration water in lysozyme as determined by NMR and predicted by MD simulations, respectively (Lagi *et al.*, 2008). Protein conformational motions and unfolding have activation energies of roughly 8–33 kJ mol^{-1} (Wolynes *et al.*, 1996; Socci *et al.*, 1996; Schuler *et al.*, 2002; Munoz *et al.*, 2006) and must also contribute to damage in this temperature range. The rough correspondence in energy between protein and solvent motions is not coincidental, because the solvent and protein dynamics are coupled (Tilton *et al.*, 1992; Wood *et al.*, 2007; Wood, Frolich *et al.*, 2008; Wood, Plazanet *et al.*, 2008). We cannot distinguish the relative contributions of these various processes in determining the observed temperature-dependence of radiation damage based upon diffraction measurements alone.

Near $T = 200$ K, the liquid-like diffusive processes (of conformational subunits and solvent) that dominate the radiation-sensitivity at higher temperatures appear to freeze out and processes with much lower activation energies dominate down to $T \simeq 100$ K. The crossover in radiation-sensitivity behavior near $T = 200$ K is consistent with previous evidence for the onset of liquid-like motions at this temperature. For example, Tilton *et al.* (1992) showed that ribonuclease A appears to have a 'dynamical transition' at $T \simeq 210$ K and this transition is associated with the appearance of enzymatic activity (Rasmussen *et al.*, 1992). A dynamical transition near $T \simeq 200$ K, manifested as a rapid increase on warming in some measures of the atomic mean-squared displacements, has also been observed for the heme iron of myoglobin (Parak *et al.*, 1982) and in the myoglobin molecule as a whole (Doster *et al.*, 1989), in purple membrane (Wood *et al.*, 2007), in maltose-binding protein (Wood, Frolich *et al.*, 2008) and in thaumatin (Warkentin & Thorne, 2009).

Below the protein-solvent glass transition, one might expect radiation damage to protein crystals to resemble radiation damage to small-molecule organic crystals, as both systems then lack significant liquid-like motions. This is indeed the case. The activation energy for the fit between $T = 200$ and 100 K in Fig. 2 is 1.00 ± 0.33 kJ mol^{-1}. Radiation-sensitivity studies of crystalline paraffin, polyethylene and L-valine have yielded activation energies between $T = 300$ and 100 K of 1.89, 1.17 and 1.71 kJ mol^{-1}, respectively (Wade, 1984). The activation energies for ovaline, coronene and metal-free phthalocynanine are ~0.8 kJ mol^{-1} (Fryer *et al.*, 1992) and the value for L-asparagine is 1.00 kJ mol^{-1} (Müller *et al.*, 2002). This agreement between such a range of different molecules suggests that the mechanisms for global damage in this 'vibrational' (as opposed to diffusive) regime are quite general.

As pointed out by Müller *et al.* (2002), the activation energy of 1.00 kJ mol^{-1} (or 10 meV) corresponds to a splitting (hf) of

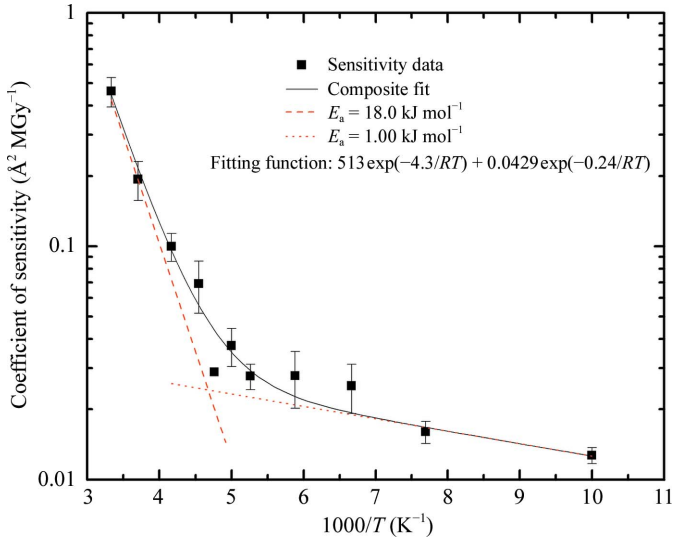

Figure 2
The coefficient of sensitivity, determined from the initial slope of data as in Fig. 1, *versus* inverse temperature for thaumatin. Each point (black square) gives the average of values from typically three or four crystals at that temperature and the error bars give the standard deviation. The solid black line is a fit to a two-activation-energy model as described in the text (1). The dashed red asymptotes indicate the individual activation energies.

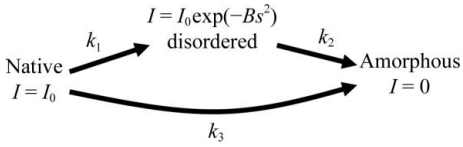

Figure 3
The radiation-damage model of Blake & Phillips (1962). An initially undamaged (native) region may become either disordered, corresponding to an increased average B factor, or amorphous, corresponding to a complete loss of Bragg scattering. Native protein can become disordered with rate constant k_1 and then completely amorphous with rate constant k_2, or it can proceed directly to the amorphous state with rate constant k_3. Present and past experiments indicate that $k_3 \simeq 0$. The rate constants determine the number of transitions per unit dose (not time) and have units of inverse dose.

vibrational energy levels with a frequency of ∼2.4 THz and is comparable to the splitting of the lowest-energy optical phonon modes in amino-acid crystals (Micu *et al.*, 1995). These modes correspond to whole-amino-acid oscillations, which are ∼10–100 times slower than the vibrations of functional groups or individual bonds (Casado *et al.*, 1995). Since this splitting is equal to the thermal energy (kT) at 115 K, quantization of these vibrational states will be important. The observed thermal activation of radiation damage could then correspond to the thermal occupancy of vibrations on the amino-acid scale, which would be common to all of the systems described above, even non-amino-acid crystals such as paraffin.

A possible mechanism by which vibrations may be coupled to radiation damage is a vibrational enhancement of reaction kinetics. Such enhancements have been observed, for example, in the dissociation kinetics of adsorbed molecules (Darling & Holloway, 1995). Below T = 100 K these high-frequency vibrations are frozen out, as shown by neutron scattering experiments at ∼50 K (Doster *et al.*, 1989), and the global radiation-sensitivity of both proteins (Borek *et al.*, 2007) and small-molecule compounds (see references above) become temperature-independent.

4.2. Modeling damage

Additional insight into the temperature-dependent nature of radiation damage can be obtained by analyzing our data using the model of Blake & Phillips (1962). Global damage to protein crystals is assumed to proceed according to the scheme presented in Fig. 3. Initially, undamaged crystal regions can become disordered at 'rate' k_1 (proportional to the number of transitions per unit dose and with units of inverse dose; Gy^{-1}). These disordered regions can then become completely amorphous at 'rate' k_2. Undamaged regions can also proceed directly to the amorphous state at 'rate' k_3. Diffraction from disordered regions is modeled as Bragg scattering with an increased B factor, whereas diffraction from amorphous regions is modeled as entirely diffuse.

Hendrickson (1976) showed that this model yields the following expression for the resolution-dependent and dose-dependent average intensity:

$$\frac{I(D,s)}{I(0,s)} = \exp[-(k_1+k_3)D] + \frac{k_1}{k_1+k_3-k_2} \times \exp(-k_2D)\{1-\exp[-(k_1+k_3-k_2)D]\} \times \exp(-Bs^2). \quad (2)$$

Here, D is the X-ray dose absorbed by the sample, s is the length of the scattering vector and B is the average B-factor increase within the disordered regions.

In reality, the actual increase in local B factor will vary from region to region and also with the dose. A more sophisticated model might then include a distribution of B factors, but the most obvious realisation of such a model cannot be distinguished from the present model using $I(D, s)$ data alone; a crystal with a small fraction of heavily disordered cells gives the same $I(D, s)$ as a crystal with a larger fraction of more lightly disordered cells. Similarly, additional states between k_1 and k_3 could be included but would yield little additional insight.

Fig. 4 shows a fit of (2) to data from a single crystal at T = 100 K. Similar fits to data from 40 crystals spanning the temperature range T = 100–300 K were performed. The data were truncated at I/I_0 = 0.3 and a resolution of ∼2.0 Å to increase the consistency between data sets. The average R^2 was 0.988 and in all cases R^2 was greater than 0.95. As in previous studies (Hendrickson, 1976; Sliz *et al.*, 2003), the constant k_3 was found to be zero, indicating that the protein first becomes disordered before becoming amorphous.

Figs. 5 and 6 show how the constants k_1 and k_2 and the disorder parameter B vary with temperature. Both constants k_1 and k_2 in Fig. 5 show two temperature regions that match those of the coefficient of sensitivity in Fig. 2. The solid lines indicate fits to a two-activation-energy model corresponding to (2). Below the protein-solvent glass transition near

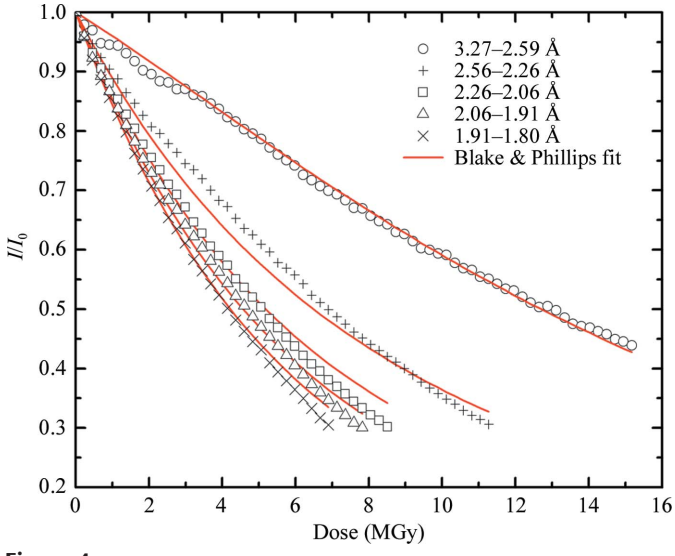

Figure 4
An example of a fit (solid lines) of (2) of the model of Blake & Phillips (1962) to diffraction data collected at T = 100 K. The diffracted intensity decreases with dose, with a more rapid decrease at larger resolutions. The three rate constants k_1, k_2 and k_3 and the disorder parameter B are extracted from the fit.

T = 200 K the activation energies for both k_1 and k_2 are the same as those obtained in Fig. 2 and the ratio k_2/k_1 is constant. However, in the liquid-like high-temperature region the constant k_2 increases with temperature more rapidly than k_1, indicating that amorphization makes a relatively larger contribution to global damage at higher temperatures. This is consistent with the notion that large-scale intra-protein and inter-protein motions, which are more likely than local motions to cause a molecule to cease contributing to ordered diffraction, are frozen out below T = 200 K and become increasingly important at higher temperatures.

The disorder parameter B in (2) is the average B factor of the disordered crystal fraction. The larger B is, the more disorder that must accumulate before a region will transition (at rate k_2) to the amorphous state. In Fig. 6, B is approximately constant between T = 100 and ∼210 K and then drops to less than half of its T = 100 K value above 210 K. This indicates that at higher temperatures less disorder/less molecular damage is required to trigger a transition to the amorphous phase; crudely, a single hit in an already damaged region may trigger a major conformational change in the protein. At low temperatures, the rigid solvent scaffold prevents such motions and the protein can sustain many more hits and become much more damaged before becoming amorphous.

Previous analyses of radiation-sensitivity data using the model of Blake and Phillips have been limited to either T = 300 or 100 K and none have reported the X-ray dose. However, some comparisons with the present results are possible. The ratio k_1/k_2 and the disorder parameter B are independent of the units of the rate constants. For myoglobin at room temperature, Hendrickson (1976) found that $k_1/k_2 \simeq 0.5$ and $B \simeq 35$ Å^2. For three proteins at T = 100 K, Sliz *et al.* (2003) obtained k_1/k_2 values in the range 1.5–2.0, compared with our value of ∼2.5 at 100 K, and B values ranging from 40 to 60 Å^2, compared with our value of ∼32 Å^2. Hendrickson also found that k_3 is zero at T = 300 K within experimental error, indicating that the process of radiation damage proceeds sequentially through the disordered state, a finding that we corroborate at all temperatures.

4.3. Other models for radiation damage

Motivated by observations of gas release when irradiated protein crystals are warmed from T = 100 K to room temperature, it has been suggested that hydrogen generated during irradiation may disproportionately contribute to radiation damage. For example, Meents *et al.* (2010) recently reported measurements of radiation damage to two proteins (insulin and elastase) at temperatures between 160 and 5 K. They conclude that hydrogen gas formed inside the sample during irradiation is mainly responsible for the loss of high-resolution information and contrast in diffraction experiments and electron microscopy, dominating over all of the radiation-damage mechanisms for this temperature range discussed here and in the previous literature.

As evidence for this interpretation, Meents and coworkers report anomalies in the unit-cell volume, mosaicity, R factors and SAXS data near T = 30 K. They suggest that at higher temperatures hydrogen can easily diffuse within the crystal and accumulate at vacancies and lattice imperfections, but that

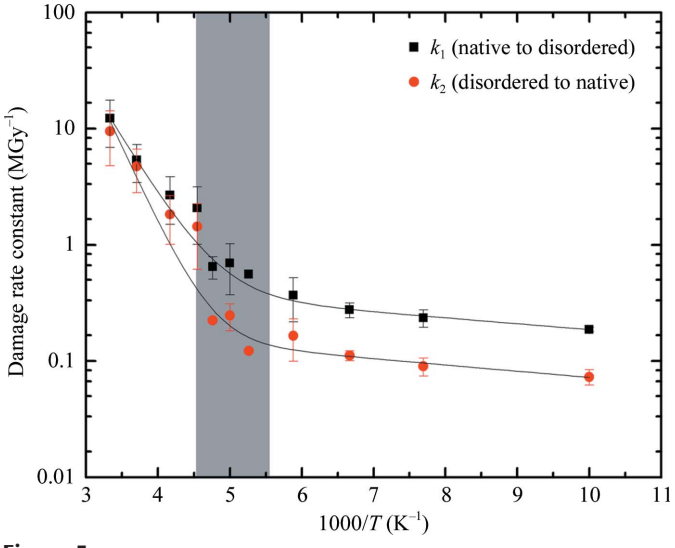

Figure 5
The rate constants k_1 and k_2, as determined from fits to (2) such as that shown in Fig. 4 *versus* inverse temperature. Symbols and error bars indicate the mean and standard deviation obtained from all crystals examined at that temperature. The solid black lines indicate two-activation-energy fits as in Fig. 2. Below $T \simeq 200$ K the activation energies for k_1 (native to disordered) and k_2 (disordered to amorphous) are the same, but above 200 K the activation energy for k_2 is almost twice that for k_1. Shading indicates the temperature range 180–220 K in which the protein glass transition is believed to occur.

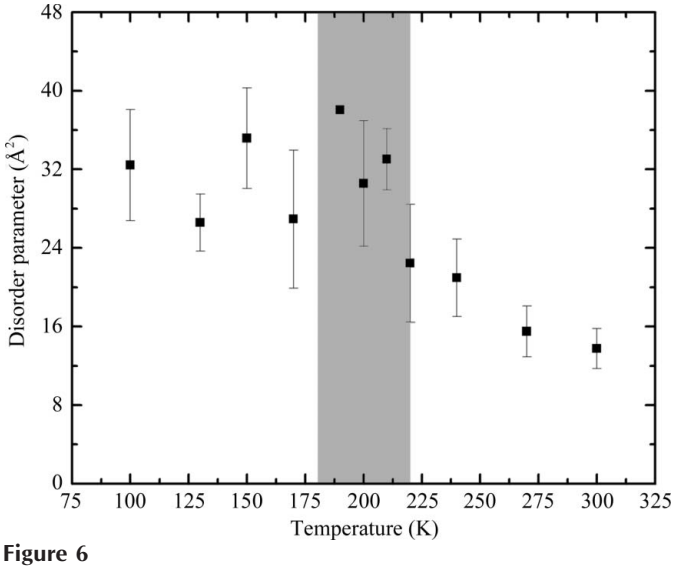

Figure 6
The disorder parameter B, corresponding to the average B factor of protein in the disordered state, *versus* temperature, as determined from fits to (2) such as that shown in Fig. 4. Shading indicates the temperature range 180–220 K in which the protein glass transition is believed to occur. The disorder parameter decreases by a factor of roughly two on warming from below the glass transition to above it. At low temperatures, the rigid solvent scaffold prevents conformational motions so that significant disorder must accumulate before the transition to the amorphous phase occurs. The liquid-like motions possible at high temperatures allow a small amount of disorder to trigger a large conformational change.

at $T = 30$ K hydrogen becomes immobile, leading to the more rapid loss of order with dose that they observe near this temperature.

Hydrogen (H_2) gas evolution from water (Nurnberger, 1937) and from organic compounds (Chapiro, 1962) upon irradiation has been studied for more than half a century. H_2 gas adsorbed to the surface of ice rapidly desorbs between $T \simeq 16$ K and $T \simeq 25$ K (Zheng *et al.*, 2006). However, H_2 gas formed in the bulk by irradiation at $T = 12$ K is not released from the surface until the ice is warmed to at least $T \simeq 90$ K, with release being complete by $\sim$140 K (Zheng *et al.*, 2006). Experiments at $T = 100$ K on irradiated H_2O films covered by a 26-monolayer-thick D_2O overlayer show that H_2 does not begin to emerge from the D_2O surface until $\sim$100 s after the start of irradiation (Petrik & Kimmel, 2004), indicating the extremely slow long-range translational diffusion of H_2 through amorphous ice even at this high temperature.

Consequently, the temperature-dependent features observed in diffraction experiments by Meents and coworkers below $T = 50$ K cannot be associated with mobile H_2. On the other hand, both the present experiments and those of Meents and coworkers cover the temperature range in which H_2 first becomes mobile and also in which it is expected to completely leave the crystal. No features are observed in any diffraction properties that can be correlated with this dramatic evolution of hydrogen mobility.

More generally, in analogy with the radiation-induced formation and diffusion of vacancy–interstitial pairs in atomic and molecular solids, there is no reason for displacements of H atoms to contribute more to crystal disorder and degradation of diffraction properties than the displacements of the atoms to which they were originally bonded. Recombination to form molecular hydrogen and diffusion of H_2 to grain boundaries (Dobrianov *et al.*, 1999) and to the crystal surface will in fact diminish the relative contribution of hydrogen.

4.4. The optimum data-collection temperature?

Cooling crystals to $T = 100$ K minimizes radiation damage and reduces the thermal contribution to B factors and so for most purposes is the best choice for collecting structural data sets. However, this cooling dramatically increases crystal mosaicities from typical as-grown values of 0.01° to 0.2–0.5° or more, which acts to decrease the achievable resolution. This mosaicity increase can be avoided by cooling crystals to $T = 220$ K, which is just above the glass transition and where the internal solvent remains liquid, and by carefully removing all external solvent prior to cooling so as to inhibit crystalline ice formation (Warkentin & Thorne, 2009). The cost is a factor of five increase in radiation-sensitivity compared with $T = 100$ K, which can be overcome by using crystals with volumes five times larger and linear dimensions 1.7 times larger. As synchrotron beamlines and data-acquisition hardware are improved to take advantage of small mosaicities, data collection at $T = 220$ K may become an increasingly attractive alternative.

5. Conclusions

Measurements of radiation-sensitivity *versus* temperature provide insight into the mechanisms of radiation damage to protein crystals and an alternative window on the protein-solvent glass transition. Above the glass transition near $T = 200$ K, the large activation energy for damage indicates that liquid-like diffusive motions within the protein and solvent dominate. Below the glass transition, a much smaller activation energy that is comparable to the values obtained from water-free small-molecule organic crystals is observed. This activation energy is comparable to the energies of vibrational quanta of amino-acid-scale vibrations, suggesting that thermal vibration-assisted reactions may dominate radiation damage below the glass transition. Consistent with this view, both these vibration amplitudes (as measured by neutron scattering) and global radiation-sensitivity are nearly temperature-independent below $T \simeq 80$ K.

Fits to the three-state model of Blake and Phillips indicate that damage proceeds sequentially, from native to disordered to amorphous states, at all temperatures. Above the glass transition, the relative importance of amorphization increases and the amount of disorder a crystal region must develop before transitioning to the amorphous state drops, indicating that radiation-damage-induced large-scale motions become increasingly important.

The present results provide detailed data necessary for optimization of data collection at all temperatures. They may be particularly useful in studies of the protein glass transition, in mechanistic studies of protein function and in the developing field of kinetic crystallography (Bourgeois & Royant, 2005; Colletier *et al.*, 2008; Weik & Colletier, 2010), in which temperature can be used as a parameter to control reaction rates within crystals.

This work was supported by the National Institutes of Health (NIH) under award No. GM065981-05 A1. It is based on research conducted at the Cornell High-Energy Synchrotron Source (CHESS), which is supported by the National Science Foundation (NSF) and the NIH/National Institute of General Medical Sciences under NSF award No. DMR-0225180, using the Macromolecular Diffraction at CHESS (MacCHESS) facility, which is supported by award No. RR-01646 from the NIH through its National Center for Research Resources.

References

Anbar, M. & Hart, E. J. (1967). *J. Phys. Chem.* **71**, 3700–3702.
Blake, C. & Phillips, D. C. (1962). *Biological Effects of Ionizing Radiation at the Molecular Level*, pp. 183–191. Vienna: IAEA.
Borek, D., Ginell, S. L., Cymborowski, M., Minor, W. & Otwinowski, Z. (2007). *J. Synchrotron Rad.* **14**, 24–33.
Bourgeois, D. & Royant, A. (2005). *Curr. Opin. Struct. Biol.* **15**, 538–547.
Burmeister, W. P. (2000). *Acta Cryst.* D**56**, 328–341.
Buxton, G. V., Greenstock, C. L., Helman, W. P. & Ross, A. B. (1988). *J. Phys. Chem. Ref. Data*, **17**, 513–886.

Casado, J., Navarrete, J. T. L. & Ramirez, F. J. (1995). *Spectrochim. Acta A*, **51**, 2347–2356.
Chapiro, A. (1962). *Radiation Chemistry of Polymeric Systems.* New York: Interscience.
Charron, C., Kadri, A., Robert, M.-C., Giegé, R. & Lorber, B. (2002). *Acta Cryst.* D**58**, 2060–2065.
Cole, A. (1969). *Radiat. Res.* **38**, 7–33.
Collaborative Computational Project, Number 4 (1994). *Acta Cryst.* D**50**, 760–763.
Colletier, J.-P., Bourgeois, D., Sanson, B., Fournier, D., Sussman, J. L., Silman, I. & Weik, M. (2008). *Proc. Natl Acad. Sci. USA*, **105**, 11742–11747.
Coulibaly, F., Chiu, E., Ikeda, K., Gutmann, S., Haebel, P. W., Schulze-Briese, C., Mori, H. & Metcalf, P. (2007). *Nature (London)*, **446**, 97–101.
Cowan, J. A. & Nave, C. (2008). *J. Synchrotron Rad.* **15**, 458–462.
Darling, G. R. & Holloway, S. (1995). *Rep. Prog. Phys.* **58**, 1595–1672.
Dobrianov, I., Caylor, C., Lemay, S. G., Finkelstein, K. D. & Thorne, R. E. (1999). *J. Cryst. Growth*, **196**, 511–523.
Doster, W., Cusack, S. & Petry, W. (1989). *Nature (London)*, **337**, 754–756.
Fryer, J. R., McConnell, C. H., Zemlin, F. & Dorset, D. L. (1992). *Ultramicroscopy*, **40**, 163–169.
Gabel, F., Bicout, D., Lehnert, U., Tehei, M., Weik, M. & Zaccai, G. (2002). *Q. Rev. Biophys.* **35**, 327–367.
Garman, E. F. (2010). *Acta Cryst.* D**66**, 339–351.
Garman, E. F. & Schneider, T. R. (1997). *J. Appl. Cryst.* **30**, 211–237.
Henderson, R. (1990). *Proc. R. Soc. London Ser. B Biol. Sci.* **241**, 6–8.
Henderson, R. (1995). *Q. Rev. Biophys.* **28**, 171–193.
Hendrickson, W. A. (1976). *J. Mol. Biol.* **106**, 889–893.
Holton, J. M. (2009). *J. Synchrotron Rad.* **16**, 133–142.
Holton, J. M. & Frankel, K. A. (2010). *Acta Cryst.* D**66**, 393–408.
Hope, H. (1988). *Acta Cryst.* B**44**, 22–26.
Howell, P. L. & Smith, G. D. (1992). *J. Appl. Cryst.* **25**, 81–86.
Juers, D. H. & Matthews, B. W. (2001). *J. Mol. Biol.* **311**, 851–862.
Juers, D. H. & Matthews, B. W. (2004). *Acta Cryst.* D**60**, 412–421.
Kmetko, J., Husseini, N. S., Naides, M., Kalinin, Y. & Thorne, R. E. (2006). *Acta Cryst.* D**62**, 1030–1038.
Kriminski, S., Caylor, C. L., Nonato, M. C., Finkelstein, K. D. & Thorne, R. E. (2002). *Acta Cryst.* D**58**, 459–471.
Lagi, M., Chu, X., Kim, C., Mallamace, F., Baglioni, P. & Chen, S.-H. (2008). *J. Phys. Chem. B*, **112**, 1571–1575.
Leiros, H.-K. S., McSweeney, S. M. & Smalås, A. O. (2001). *Acta Cryst.* D**57**, 488–497.
Leiros, H.-K. S., Timmins, J., Ravelli, R. B. G. & McSweeney, S. M. (2006). *Acta Cryst.* D**62**, 125–132.
Leslie, A. G. W. (2006). *Acta Cryst.* D**62**, 48–57.
Meents, A., Gutmann, S., Wagner, A. & Schulze-Briese, C. (2010). *Proc. Natl Acad. Sci. USA*, **107**, 1094–1099.
Micu, A. M., Durand, D., Quilichini, M., Field, M. J. & Smith, J. C. (1995). *J. Phys. Chem.* **99**, 5645–5657.
Müller, R., Weckert, E., Zellner, J. & Drakopoulos, M. (2002). *J. Synchrotron Rad.* **9**, 368–374.
Munoz, V., Ghirlando, R., Blanco, F. J., Jas, G. S., Hofrichter, J. & Eaton, W. A. (2006). *Biochemistry*, **45**, 7023–7035.
Nave, C. & Garman, E. F. (2005). *J. Synchrotron Rad.* **12**, 257–260.
Nave, C. & Hill, M. A. (2005). *J. Synchrotron Rad.* **12**, 299–303.
Nurnberger, C. E. (1937). *J. Phys. Chem.* **41**, 431–435.
Otwinowski, Z. & Minor, W. (1997). *Methods Enzymol.* **276**, 307–326.
Owen, R. L., Rudino-Pinera, E. & Garman, E. F. (2006). *Proc. Natl Acad. Sci. USA*, **103**, 4912–4917.
Parak, F., Knapp, E. W. & Kucheida, D. (1982). *J. Mol. Biol.* **161**, 177–194.
Petrik, N. G. & Kimmel, G. A. (2004). *J. Chem. Phys.* **121**, 3736–3744.
Rasmussen, B. F., Stock, A. M., Ringe, D. & Petsko, G. A. (1992). *Nature (London)*, **357**, 423–424.
Rault, J., Neffati, R. & Judeinstein, P. (2003). *Eur. Phys. J. B*, **36**, 627–637.
Ravelli, R. B. G., Leiros, H.-K. S., Pan, B., Caffrey, M. & McSweeney, S. (2003). *Structure*, **11**, 217–224.
Ravelli, R. B. G. & McSweeney, S. M. (2000). *Structure*, **8**, 315–328.
Ravelli, R. B. G., Nanao, M. H., Lovering, A., White, S. & McSweeney, S. (2005). *J. Synchrotron Rad.* **12**, 276–284.
Ravelli, R. B. G., Theveneau, P., McSweeney, S. & Caffrey, M. (2002). *J. Synchrotron Rad.* **9**, 355–360.
Rodgers, D. W. (1994). *Structure*, **2**, 1135–1140.
Schlichting, I., Berendzen, J., Chu, K., Stock, A. M., Maves, S. A., Benson, D. E., Sweet, B. M., Ringe, D., Petsko, G. A. & Sligar, S. G. (2000). *Science*, **287**, 1615–1622.
Schuler, B., Lipman, E. A. & Eaton, W. A. (2002). *Nature (London)*, **419**, 743–747.
Shimizu, N., Hirata, K., Hasegawa, K., Ueno, G. & Yamamoto, M. (2007). *J. Synchrotron Rad.* **14**, 4–10.
Singh, A. & Singh, H. (1982). *Prog. Biophys. Mol. Biol.* **39**, 69–107.
Sliz, P., Harrison, S. C. & Rosenbaum, G. (2003). *Structure*, **11**, 13–19.
Socci, N. D., Onuchic, J. N. & Wolynes, P. G. (1996). *J. Chem. Phys.* **104**, 5860–5868.
Southworth-Davies, R. J., Medina, M. A., Carmichael, I. & Garman, E. F. (2007). *Structure*, **15**, 1531–1541.
Teng, T. & Moffat, K. (2000). *J. Synchrotron Rad.* **7**, 313–317.
Teng, T.-Y. & Moffat, K. (2002). *J. Synchrotron Rad.* **9**, 198–201.
Tilton, R. F., Dewan, J. C. & Petsko, G. A. (1992). *Biochemistry*, **31**, 2469–2481.
Wade, R. H. (1984). *Ultramicroscopy*, **14**, 265–270.
Warkentin, M., Berejnov, V., Husseini, N. S. & Thorne, R. E. (2006). *J. Appl. Cryst.* **39**, 805–811.
Warkentin, M. & Thorne, R. E. (2009). *J. Appl. Cryst.* **42**, 944–952.
Weik, M. & Colletier, J.-P. (2010). *Acta Cryst.* D**66**, 437–446.
Weik, M., Kryger, G., Schreurs, A. M. M., Bouma, B., Silman, I., Sussman, J. L., Gros, P. & Kroon, J. (2001). *Acta Cryst.* D**57**, 566–573.
Weik, M., Ravelli, R. B. G., Kryger, G., McSweeney, S., Raves, M. L., Harel, M., Gros, P., Silman, I., Kroon, J. & Sussman, J. L. (2000). *Proc. Natl Acad. Sci. USA*, **97**, 623–628.
Weik, M., Schreurs, A. M. M., Leiros, H.-K. S., Zaccai, G., Ravelli, R. B. G. & Gros, P. (2005). *J. Synchrotron Rad.* **12**, 310–317.
Weik, M., Vernede, X., Royant, A. & Bourgeois, D. (2004). *Biophys. J.* **86**, 3176–3185.
Wolynes, P. G., Luthey-Schulten, Z. & Onuchic, J. N. (1996). *Chem. Biol.* **3**, 425–432.
Wood, K., Frolich, A., Paciaroni, A., Moulin, M., Hartlein, M., Zaccai, G., Tobias, D. J. & Weik, M. (2008). *J. Am. Chem. Soc.* **130**, 4586–4587.
Wood, K., Plazanet, M., Gabel, F., Kessler, B., Oesterhelt, D., Tobias, D. J., Zaccai, G. & Weik, M. (2007). *Proc. Natl Acad. Sci. USA*, **104**, 18049–18054.
Wood, K., Plazanet, M., Gabel, F., Kessler, B., Oesterhelt, D., Zaccai, G. & Weik, M. (2008). *Eur. Biophys. J.* **37**, 619–626.
Zheng, W., Jewitt, D. & Kaiser, R. I. (2006). *Astrophys. J.* **648**, 753–761.